ACS APPLIED POLYMER MATERIALS

pubs.acs.org/acsapm

Article

Silicon Doping by Polymer Grafting: Size Distribution Matters

Michele Perego,* Stefano Kuschlan, Gabriele Seguini, Riccardo Chiarcos, Valentina Gianotti, Diego Antonioli, Katia Sparnacci, and Michele Laus*

Cite This: *ACS Appl. Polym. Mater.* 2021, 3, 6383−6393

Read Online

ACCESS | Metrics & More | Article Recommendations | Supporting Information

ABSTRACT: Phosphorus δ-layers in SiO_2 have been prepared by means of poly(methyl methacrylate) (PMMA), terminated with a phosphorus-containing moiety acting as an anchoring group. In particular, grafting of two P-terminated PMMA samples with M_n = 7.5 kg/mol ($Đ$ = 1.14) and M_n = 17.8 kg/mol ($Đ$ = 1.23) onto 10 nm thick SiO_2 films deposited on Si substrates has been investigated, focusing on the thickness evolution of the brush layer as a function of the processing parameters, that is, annealing temperature and time. Upon removal of the polymer chains and subsequent encapsulation into a SiO_2 matrix, the concentration of phosphorus atoms into the P δ-layers has been monitored by time-of-flight secondary ion mass spectrometry. The effective P dose in the P δ-layer is mainly dictated by the molecular weight of the P-terminated PMMA, and the doping process results are highly reproducible, provided that tight control over the experimental protocol is granted. However, although the grafting density is expected to progressively increase as a function of annealing time with a linear correlation between grafting density and thickness, the measured P dose in the δ-layers is observed to follow the opposite trend. This effect has been accounted for by considering a distortion of the molecular weight distribution of the grafted species with respect to the initial molecular weight distribution of the polymer. The overall picture reveals important information about the mechanism and dynamics governing the "grafting to" process of P-terminated PMMA polymers onto nondeglazed Si substrates.

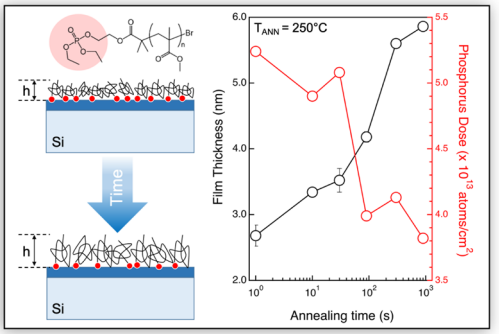

KEYWORDS: *doping, silicon, polymers, phosphorus, activation, self-assembled monolayers*

INTRODUCTION

Surface design represents a fundamental research topic in different disciplines and self-assembled monolayers (SAMs) of molecules have been widely investigated in nanotechnology to modify the surface properties and engineer the active elements in biosensors,[1] catalysis,[2] biomedical devices,[3] solar cells,[4] and thin-film transistors.[5] In order to ensure long-term stability of the modified surfaces, covalent bonding of the molecules forming the SAM is commonly preferred over simple layer deposition by physisorption. Silanes, thiols, carboxylic acids, and alkenes have suitable anchor groups for grafting to metal and semiconductor surfaces depending on the complementary surface functional groups. Organophosphonates have been reported as a versatile solution to form stable SAM on a broad class of semiconductor and dielectric surfaces, with potential applications on several different nanostructures and novel emerging materials as well.[6] Organophosphonate chemistry has attracted a growing interest because SAM formation does not require tight control of environmental conditions and the strong phosphonate-oxide bond guarantees stable anchoring of the molecules over the substrate.[7−10] The stability of organophosphonate interfaces on technologically relevant semiconductors has been widely investigated, providing important insights into the parameters that govern their grafting and organization over the surface.[6,11−15]

In particular, SAMs of organophosphonates have been proposed as a viable and mild solution for the ex situ doping of a large variety of semiconductor materials.[11,15−17] Doping of 2D materials, such as graphene, has been achieved using SAM of organophosphates. For instance, arylphosphonic acids have been used to engineer the electronic properties of atomically thin sheets of semiconducting transition-metal dichalcogenides.[18] Doping of silicon and other bulk semiconductors has been achieved by means of SAM of P-containing molecules in the so called monolayer doping approach.[15,16,19−21] This approach relies on the formation of a SAM over the semiconductor surface and subsequent injection of the dopant into the substrate by a high-temperature thermal treatment. The described procedure has been used to enable the

Received: September 6, 2021
Accepted: November 2, 2021
Published: November 11, 2021

formation of sub 5 nm ultrashallow junctions in Si.[16,17] Interesting exploitation perspectives are also expected for photovoltaic applications, which usually require effective approaches to reduce the cost of the devices.[22] Further developments of this doping approach have been recently proposed by bonding a diethylphosphate group to a 2-hydroxyethyl(isobutyrate) moiety at one end of polystyrene (PS) or polymethyl methacrylate (PMMA) chains.[23] The dopant-containing moieties have been used to graft the polymers to an activated Si substrate and form a brush layer. The grafting process has been efficiently implemented on both nondeglazed and deglazed Si substrate, that is, on silicon samples covered by a thin native oxide film or treated in hydrofluoric acid solution to chemically remove the SiO_2 layer, leaving a hydrogen-terminated Si surface. In this respect, hydrofluoric acid deglazed surfaces represent nonmanufacturing-friendly semiconducting substrates. Conversely, the possibility to operate on SiO_2 is highly desirable for industrial upscaling of the process because SiO_2 is ubiquitous in semiconducting devices, at least in the form of native oxide on Si surfaces.[24−26] In principle, for "grafting to" reactions, the grafting density of macromolecules in the brush layer depends on the gyration radius of the polymer and can be properly tuned by changing the degree of polymerization of the functional polymer.[27,28] Actually, the total dose of phosphorus deposited onto the nondeglazed Si substrate has been shown to well correlate with the degree of polymerization of the polymers terminated with the P-containing moiety.[27] Simple and efficient removal of the polymeric chains has been achieved by O_2 plasma, without affecting the tethered P-containing moieties on the surface. A cumulative and stepwise increase in the dose of P atoms grafted to the silicon surface is demonstrated by simple iteration of grafting/ashing cycles.[27,29,30] Upon deposition of a SiO_2 layer to prevent P outgassing, P atoms were efficiently injected into the Si substrate by high-temperature thermal treatments, demonstrating high activation rates (80%) of injected P atoms.[29] From this point of view, the proposed doping technology present several advantages compared to other polymer-assisted doping approaches that have been proposed by other groups in the literature.[31−34] In particular, the self-limiting nature of the brush layer formation guarantees a more accurate and reliable control over the dose of phosphorus atoms in the dopant source and a precise localization of the source with P atoms forming a δ-layer embedded into the SiO_2 matrix with negligible carbon contaminations.

In general, polymer chains terminated with phosphorus-containing molecules acting as anchor groups for grafting to the target surface have been reported as a viable solution for the functional modification of surfaces.[35−37] Because of their technological interest, "grafting to" processes of polymers over a substrate have been widely investigated in the literature. However, polymer-solid substrate reactions are far more complex than the analogous reactions involving small-molecule reactants because the polymer grafting process is influenced by both steric and thermodynamic factors.[38] Usually, the "grafting to" process is reported to be self-limiting because when the grafting density increases, the energy gained by bonding a new chain to the surface is expected to be offset by the entropic cost of introducing another chain into the brush layer.[39] Actually, in a recent paper, Laus et al. demonstrated that in the case of hydroxy-terminated statistical copolymers, a mechanochemical control of the reaction determines the self-limiting nature of this process rather than a simple energy gain/entropic cost balance.[40] Moreover, recent experimental results highlighted that a substantial partitioning according to the molecular weight takes place during the "grafting to" process of a relatively polydisperse sample onto an interface, with shorter chains being preferentially attached.[41,42] This variation in the molecular weight distribution with respect to the original polymer sample could significantly impact on the grafting density of the polymers tethered to the substrate. In the specific case of polymers terminated with phosphorus-containing molecules, these results suggest that the number of macromolecules that are grafted to the substrate and, consequently, the total dose of phosphorus that is localized onto the nondeglazed Si substrate is not fully controlled by selecting the molecular weight of the P-terminated polymers that are used to form the brush layer. This capability to control the dose of P atoms by the molecular weight of the P-terminated polymer has been assumed as the cornerstone for the development of an alternative protocol for the doping of semiconductors. Deviations from this fundamental assumption imply a reduction in the level of accuracy associated to this doping strategy and need to be accurately understood in order to develop a reliable protocol for the doping of semiconductors.

In this work, the grafting onto the nondeglazed Si substrate of two phosphorus end-terminated PMMA samples (PMMA-P) having different molecular weights and narrow polydispersity has been investigated. In particular, the thickness evolution of the brush layer has been followed as a function of the processing parameters, that is, annealing temperature and time, while independent monitoring of the concentration of P atoms into the δ-layer and the average molecular weight of the PMMA-P chains in the brush layer was carried out. Collected data have been discussed in view of the integration of these P-terminated polymers in advanced protocols for the doping of semiconductors.

EXPERIMENTAL SECTION

Materials. Two hydroxy-terminated polymethylmethacrylate samples (PMMA-OH) were synthesized by activators regenerated by electron transfer-atom transfer radical polymerization (ARGET-ATRP) following the standard procedure that has been already described in a previous publication.[27] 2-Hydroxyethyl(2-bromoisobutyrate) (HEBIB) was employed as the initiator, $CuBr_2$/tris(2-pyridylmethyl)-amine (TPMA) as the catalyst, and tin(II) 2-ethylhexanoate [$Sn(EH)_2$] as the reducing agent. The initial ratios $[HEBIB]_0/[CuBr_2]_0/[TPMA]_0/[Sn(EH)_2]_0$ were fixed at the values of 1/0.04/0.24/0.2. The ratio $[MMA]_0/[HEBIB]_0$ was fixed at 30 and 250 for the two PMMA-OH polymers. The reactions were carried out at 70 °C for 45 min and 2 h, respectively. After purification of the samples by repeated precipitations from tetrahydrofuran (THF) to methanol, both PMMA-OH samples were reacted with diethyl chlorophosphate following the synthetic procedure previously described[23,27] to form diethylphosphate-terminated polymethylmethacrylate samples (PMMA-P) with quantitative yield of the phosphorylation reaction as reported in detail in the Supporting Information. The PMMA-OH and PMMA-P polymers were characterized by size-exclusion chromatography (SEC), employing a 590 Waters chromatograph equipped with Waters HSPgel HR3 and HR4 columns (0.3 mL·min^{-1}, THF as eluent) and a refractive index detector. Number-average molecular weight (M_n) and polydispersity index ($Đ$) values were obtained by the analysis of SEC data. In order to obtain information about the chemical structure of the PMMA-OH and PMMA-P polymers, ^{1}H NMR, ^{13}C NMR, and ^{31}P NMR analysis were performed with a 500 MHz (Bruker) NMR spectrometer.

https://doi.org/10.1021/acsapm.1c01157
ACS Appl. Polym. Mater. 2021, 3, 6383−6393

Substrate Preparation and Cleaning. A 4″ p-type Czochralski-grown Si(100) wafer was used as a substrate. Nominal resistivity of the substrate is 1−5 Ω cm. The removal of the native SiO_2 film was accomplished by diluted hydrofluoric acid (HF and H_2O in 1:50 ratio). Samples were immersed in solution for 1 min and rinsed in deionized H_2O for 2 min. The wafer was subsequently dried under N_2 flow and immediately loaded in the deposition chamber of an evaporator system operating at a base pressure of $P \sim 5 \times 10^{-7}$ mbar. The procedure was optimized in order to minimize wafer exposure to air. A SiO_2 layer was deposited by e-beam evaporation on the Si substrate. Deposition rate of the SiO_2 film was in situ monitored by a quartz microbalance and the evaporation conditions were adjusted to deposit a ∼10 nm thick SiO_2 film. Ex situ ellipsometry was used to determine the effective thickness of the evaporated SiO_2 layer. In the following sections, we will refer to these substrates as the nondeglazed Si substrate. Before starting the doping process, the wafer was cleaved in 1 × 1 cm^2 Si pieces that were cleaned in Piranha solution (H_2SO_4 and H_2O_2 in a 3:1 ratio) at 80 °C for 40 min to remove all organic impurities and increase the surface density of hydroxyl groups. Upon rinsing with deionized water for 3 min, the Si pieces were finally dried under N_2 flow.

P δ-Layer Synthesis. A solution with 18.0 mg of PMMA-P dissolved into 2.00 mL of toluene was spin-casted on the 1 × 1 cm^2 samples. PMMA-P concentration in the toluene solution is ∼1 wt %. This value is well within the limits reported by Lundy et al. for a uniform monolayer coverage, ruling out the hypothesis of inhomogeneous surface coverage due to the formation of agglomerates over the substrate during the spin-coating process or subsequent thermal treatment.[43] Spin-casting parameters (3000 rpm, 30 s) were adjusted to form 30 nm thick polymer films. To promote the grafting reaction, the samples were annealed at temperatures ranging from 190 to 270 °C using a rapid thermal processing (RTP) apparatus (Jipelec Jet-First Series) in an ultrapure N_2 atmosphere.[44] Upon annealing, unreacted PMMA-P chains were removed by sonication in toluene for 5 min, and the resulting solutions were kept for matrix-assisted laser desorption/ionization-time of flight (MALDI-TOF) analysis. Finally, the substrates were dried under a N_2 flow. Spectroscopic ellipsometer measurements were performed to constantly monitor the thicknesses of the as-spun polymer films and of the resulting grafted layers. Tethered polymer chains were removed by a simple treatment in O_2 plasma. Complete removal of the brush layer was obtained by accurate tuning of the O_2 plasma treatment. Experimental results demonstrated that the O_2 plasma treatment does not affect the concentration of P-containing molecules on the substrate. Finally, the P atoms were encapsulated into a SiO_2 matrix by e-beam evaporation of a 15 nm thick SiO_2 capping layer. A scheme providing a pictorial description of the process is reported in a previous work published by Perego et al.[27] The thicknesses of the top and bottom SiO_2 layers were properly adjusted in order to position the P δ-layer approximately in the middle of the SiO_2 matrix at reasonable distances from the sample surface and from the SiO_2/Si interface. In this way, it was possible to rule out any matrix effect that could modify secondary ion signals during ToF-SIMS analysis and guarantee an accurate measurement of the P-areal dose without affecting the chemistry of the grafting process that is performed on a surface fully equivalent to the one of a nondeglazed silicon substrate. The protocol for the sample preparation has been fully described in a previous publication.[27] It is worth to note that for each brush layer, that is, for each combination of annealing temperature and time, we produced two different samples that were processed using the same recipe. In addition, to further verify the accuracy and reliability of the experimental results, the sets of samples processed in RTP for 900 s at different temperatures were reproduced for both PMMA-$P_{7.5}$ and PMMA-$P_{17.8}$.

Polymer Film Characterization. Thicknesses of spin-casted polymer films before and after thermal treatment as well as of the layer of tethered polymers were determined by means of an M-200 U spectroscopic ellipsometer (J.A. Wollam Co. Inc.). Ellipsometric spectra were recorded at 70° fixed angle over the wavelength range from 250 to 1000 nm. A xenon lamp was used to generate the incident light beam. The experimental data were fitted by means of the EASE software package 2.3 version. To determine film thickness and refractive index of the polymer film, the sample structure was modeled using a film stack composed of a silicon substrate, a ∼10 nm thick SiO_2 film, and a simple Cauchy layer model for the polymer film. Before spin-coating the polymer films, the effective thickness and refractive index of the oxide film on each sample were routinely measured. This experimental procedure reduced the number of free parameters in the model used for the fitting of the film stack and increased the accuracy of the thickness measurement. The thickness of the brush layers was determined modeling the layer of PMMA-P chains tethered to the SiO_2 surface by a standard Cauchy model and assuming a refractive index value equivalent to the one measured in the as-deposited 30 nm thick PMMA-P films. The accuracy of the thickness measurement protocol was verified by comparing results obtained by ellipsometry with X-ray reflectometry data acquired on selected test samples. To verify the homogeneity of the tethered polymer layers, the thickness of the brush layers was measured by spectroscopic ellipsometer in different points. The homogeneity of the PMMA films over the substrate before and after annealing in RTP as well as after subsequent removal of the unreacted chain by sonication in toluene was further verified by scanning electron microscopy (SEM) analysis (Zeiss Supra 40 SEM) in order to disclose any evidence of polymer agglomeration phenomena.

ToF-SIMS Analysis. Time-of-flight secondary ion mass spectrometry (ToF-SIMS) was used to obtain calibrated phosphorus depth profiles. Analysis was performed using a dual-beam IONTOF IV system operating in the negative mode. In particular, a high-energy low-current ion gun was used for the analysis and a low-energy high-current ion gun was used for sputtering. Sputtering was accomplished by Cs^+ ions at 1 keV and 100 nA, rastering over a 300 × 300 μm^2 area. Ga^+ ions at 25 keV and 2 pA were used for analysis. Secondary ion signals were generated rastering over a 50 × 50 μm^2 area that was localized in the center of the sputtering crater was determined using A 20 nm thick SiO_2 film thermally grown on a Si(100) substrate and was used as a reference to determine the sputter velocity in the SiO_2 matrix. Accordingly, assuming a constant sputter rate into the e-beam evaporated SiO_2 layers, sputter time was converted into a depth scale. Accurate calibration of the P signals in the Si matrix was performed to obtain P concentration profiles, following an analytical protocol that is widely described in previous publications.[45,46] The areal dose of P atoms in the δ-layers was determined from the P concentration profiles by simple integration of the calibrated P profiles. For each sample, at least three different ToF-SIMS depth profiles were acquired, and the P areal dose was calculated as the average of the different measurements.

MALDI-TOF Analysis. Mass distribution of the PMMA-P chains in the brush layer was investigated by MALDI-TOF analysis. The unreacted chain solutions were dried under vacuum and then dissolved again in 15 μL of the matrix/cationizing agent solution. The matrix/cationizing agent solution was obtained mixing a *trans*-2-[3-(4-*tert*-butylphenyl)-2-methyl-2-propenylidene]malonitrile solution (20 mg/mL in THF) and a NaTFA solution (0.1 M in THF) in the volume ratio 50:2. A drop (0.5 μL) of the final mixture was then deposed onto the sample plate and dried on air. MALDI-TOF analysis was performed using a Bruker ultrafleXtreme instrument equipped with a solid-state Smartbeam2 laser. All the analyses were conducted on positive ions in the linear mode, employing an accelerating voltage of 20 kV and a delay time of 250 ns. The laser power was fixed at the 40% of the maximum in all experiments, slightly above the detection threshold. Each collected spectrum was an average of 1000 laser shots. For each sample, 10 spectra were collected in different positions of the sample plate spot and added together. The raw data were then processed with the FlexAnalysis (version 3.4) software.

RESULTS

Material Characterization. Two hydroxy-terminated PMMA polymers (PMMA-OH) with different molecular

https://doi.org/10.1021/acsapm.1c01157
ACS Appl. Polym. Mater. 2021, 3, 6383−6393

weights were synthesized by ARGET-ATRP using the functional initiator HEBIB. PMMA-OH samples were then reacted with diethyl chlorophosphate to obtain diethylphosphate end-terminated PMMA polymers (PMMA-P).

Figure 1 reports the SEC chromatograms of both PMMA-OH and PMMA-P samples. All samples are characterized by a

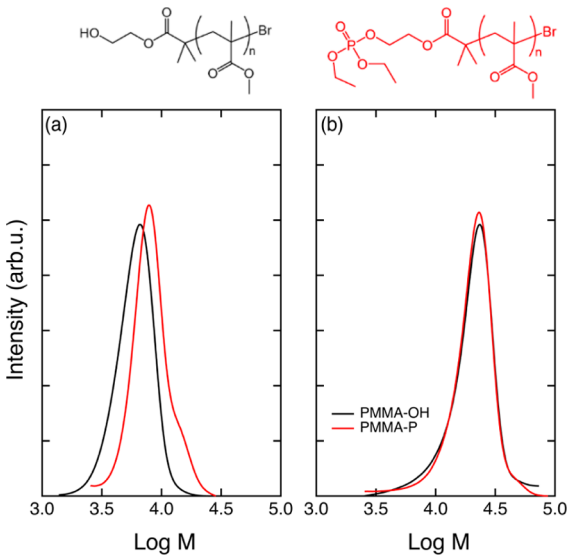

Figure 1. SEC chromatograms of PMMA-OH (black curve) and of the corresponding PMMA-P_n (red curve) samples, in the case of the low (a) and high (b) molecular weight PMMA, respectively. The chemical structures of the hydroxy-terminated and diethylphosphate end-terminated PMMA species are reported as well.

monomodal and relatively narrow molecular weight distribution. The number average molecular weights (M_n) of the two PMMA-OH samples result 5.6 kg/mol and 17.9 kg/mol. Accordingly, PMMA-OH samples were marked as PMMA-$OH_{5.6}$ and PMMA-$OH_{17.9}$. Similarly, M_n of the corresponding PMMA-P samples is 7.5 and 17.8 kg/mol, and the PMMA-P samples were labeled as PMMA-$P_{7.5}$ and PMMA-$P_{17.8}$. The slight shift toward the high-molecular-weight region of the SEC curves of the PMMA-P samples with respect to the corresponding PMMA-OH samples is probably due to the purification procedure by precipitation after the phosphorylation reaction. ^{1}H NMR, ^{13}C NMR, and ^{31}P NMR spectra were recorded for both the PMMA-OH and the PMMA-P samples. A quantitative yield of the phosphorylation reaction was confirmed for both the PMMA-$P_{7.5}$ and PMMA-$P_{17.8}$ by ^{13}C NMR analysis.

As a typical example, Figure 2 reports the ^{1}H NMR spectrum of sample PMMA-$P_{7.5}$ together with the signal assignments. From the intensities of signals c and e corresponding to the methoxy groups of the methylmethacrylate unit and the methylene group in the dimethylphosphate terminal unit, M_n of PMMA-$P_{7.5}$ can be estimated and results 7.9 kg/mol, very close to the SEC value of 7.5 kg/mol, thus confirming the proposed structure. The presence of a single signal in the ^{31}P NMR spectrum of PMMA-$P_{7.5}$ (Figure S3) as well as PMMA-$P_{17.8}$ indicates that only one P-containing moiety is present. A more detailed analysis of the NMR spectra is reported in the Supporting Information. Table 1 collects M_n and polydispersity index ($Đ$) of all the samples together with the corresponding degree of polymerization (N) and gyration radius (R_G) of the random coil configuration, estimated

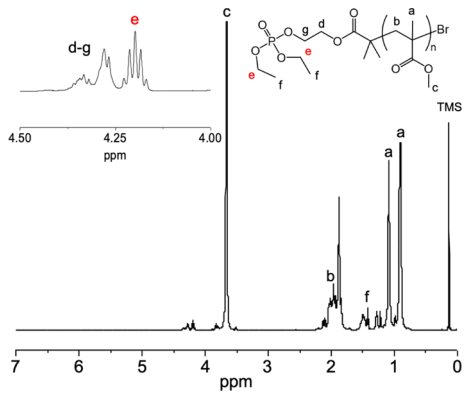

Figure 2. ^{1}H NMR spectrum of sample PMMA-$P_{7.5}$.

Table 1. Number-Average Molecular Weight (M_n), Polydispersity Index ($Đ$), Degree of Polymerization (N), and Gyration Radius (R_G) of Hydroxy-Terminated and Diethylphosphate-Terminated PMMA Polymers

sample	M_n (kg/mol)	$Đ$	N	R_G (nm)
PMMA-$OH_{5.6}$	5.6	1.13	54	2.1
PMMA-$OH_{17.9}$	17.9	1.24	177	3.8
PMMA-$P_{7.5}$	7.5	1.14	72	2.4
PMMA-$P_{17.8}$	17.8	1.23	175	3.8

considering the molecular weight of the repeat unit of PMMA (M_{MMA} = 100.121 g/mol) and the average statistical segment length b = 0.69 nm for the configurational arrangement of unperturbed PMMA chains in a melt.[47]

Grafting Kinetics. The grafting kinetic of the PMMA-$P_{7.5}$ and PMMA-$P_{17.8}$ polymers as a function of annealing temperature and time was monitored by measuring the thickness of the brush layer upon removal of unreacted chains using a spectroscopic ellipsometer. Routine SEM inspection of the samples upon spin-coating and annealing revealed a perfectly homogeneous coverage of the substrate with no evidence of polymer agglomeration (Figure S6), assuring a correct fitting of the ellipsometric data with a simple Cauchy model. Figure 3 shows the thickness evolution of the brush layers obtained by grafting the PMMA-$P_{7.5}$ (black symbols) and PMMA-$P_{17.8}$ (red symbols) polymers onto the non-deglazed Si substrates by annealing the samples for 900 s at temperatures T_{ANN} ranging from 190 to 270 °C. The black and red dashed lines indicate the thickness values equivalent to $2R_G$ for the PMMA-$P_{7.5}$ and PMMA-$P_{17.8}$, respectively. The thickness of the brush layer for PMMA-$P_{7.5}$ progressively increases when increasing the processing temperature, achieving a maximum value of 5.9 ± 0.1 nm at T_{ANN} = 250 °C. No further increment of the brush layer thickness takes place when the annealing temperature is increased at 270 °C, suggesting that the pseudo-plateau value $H \sim 6$ nm corresponds to the saturation condition. The thickness of the brush layer obtained by grafting PMMA-$P_{17.8}$ onto the Si substrates displays a similar temperature dependence with a pseudo-plateau value $H \sim 9.5$ nm. Actually, these H values correspond to ~2.5 times the R_G of the PMMM-$P_{7.5}$ and PMMA-$P_{17.8}$, suggesting that the polymer chains in the brush layer are slightly stretched, in perfect agreement with data in the literature.[48−52] This stretching of the polymer chain when reaching the pseudo-plateau value indicates that the polymer chains interact with each other, justifying the use of the term

https://doi.org/10.1021/acsapm.1c01157
ACS Appl. Polym. Mater. 2021, 3, 6383−6393

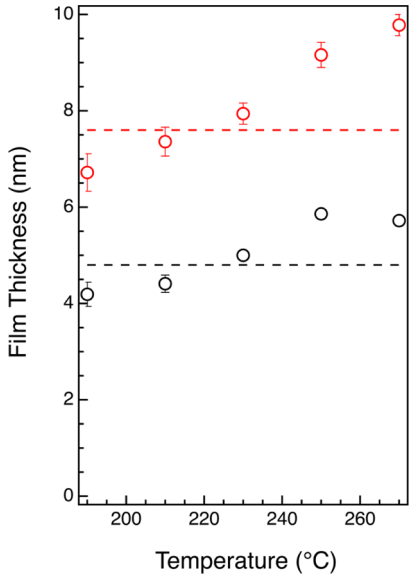

Figure 3. Thickness evolution of the brush layers obtained by grafting the PMMA-$P_{7.5}$ (black symbols) and PMMA-$P_{17.8}$ (red symbols) onto the not deglazed Si substrates. The samples were annealed for 900 s at temperatures T_{ANN} ranging from 190 to 270 °C and subsequently washed in toluene to remove unreacted chains. The black and red dashed lines indicate the thickness values equivalent to $2R_G$ for PMMA-$P_{7.5}$ and PMMA-$P_{17.8}$, respectively.

"polymer brush", that, strictly speaking, usually describes a dense array of polymer chains. Actually, polymer systems with a lower grafting density are also often denoted as "polymer brush" in the literature.[53] For this reason, the term "brush layer" will be used to refer to all the films formed by the grafted polymer chains irrespective of their dense grafting conformations.

Figure 4a,b reports the brush layer thickness evolution as a function of the annealing time (t_{ANN}) for PMMA-$P_{7.5}$ and PMMA-$P_{17.8}$, respectively. Both samples were processed at 210 °C (black symbol) and 250 °C (red symbol), without any evidence of thermal degradation, consistently with the

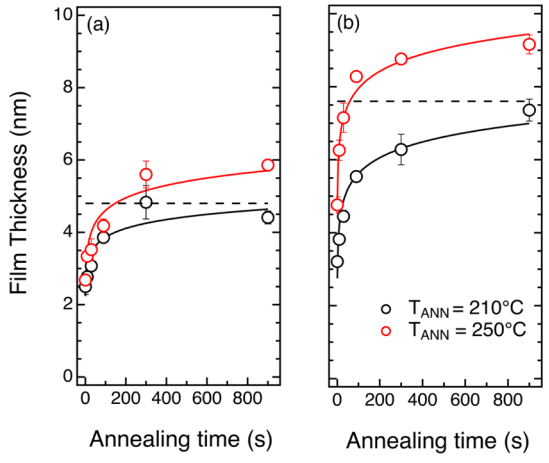

Figure 4. Brush layer thickness evolution as a function of the annealing time (t_{ANN}) for PMMA-$P_{7.5}$ (a) and PMMA-$P_{17.8}$ (b) samples, respectively. Samples were processed at 210 °C (black symbol) and 250 °C (red symbol). Solid lines are only a guide for the eye. The black dashed lines indicate the thickness values equivalent to $2R_G$ for PMMA-$P_{7.5}$ and PMMA-$P_{17.8}$, respectively.

relatively high thermal stability reported in the literature for PMMA.[54,55] At T_{ANN} = 250 °C, both samples exhibit a progressive increase in the brush layer thickness, achieving a pseudo-plateau value at t_{ANN} = 900 s. Conversely, in both cases, when annealed at T_{ANN} = 210 °C, the brush layer thickness does not reach the pseudo-plateau value H in the range of the explored t_{ANN} values. This slow evolution of the brush layer thickness is tentatively ascribed to the reduced mobility of the polymer chains in the PMMA-P films annealed at T_{ANN} = 210 °C.

Phosphorus Quantification. After the formation of the brush layer, polymer chains were removed by O_2 plasma and a 10 nm thick SiO_2 film was deposited by e-beam evaporation as a capping layer to form P δ-layers embedded into a SiO_2 matrix according to the experimental protocol that is reported by Perego et al.[27] Representative ToF-SIMS calibrated profiles of the different P δ-layers obtained with a 900 s long thermal treatment at different processing temperatures T_{ANN} are shown in Figure 5a,b for the PMMA-$P_{7.5}$ and PMMA-$P_{17.8}$ samples,

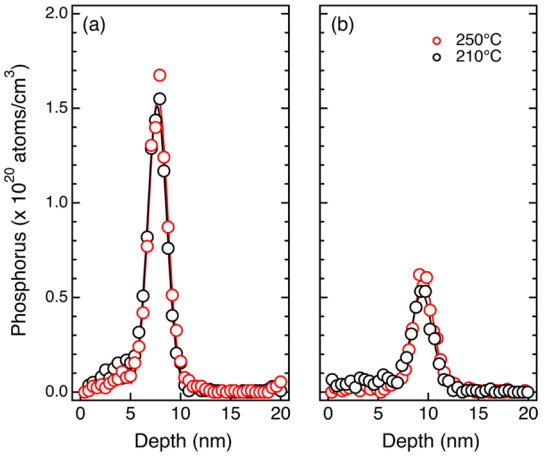

Figure 5. Representative ToF-SIMS calibrated profiles of the P δ-layers obtained with a 900 s long thermal treatment at different processing temperatures T_{ANN} for the PMMA-$P_{7.5}$ (a) and PMMA-$P_{17.8}$ (b) samples, respectively. Continuous lines correspond to the Gaussian fitting of the experimental data.

respectively. The P profiles are almost perfectly symmetric, indicating that no physisorbed P impurity atoms were left on the sample surface.[25] By integrating the ToF-SIMS calibrated profiles, the effective areal dose of P atoms in the δ-layers was calculated.

P areal doses (closed black symbols) are reported in Figure 6a,b as a function of T_{ANN} for PMMA-$P_{7.5}$ and PMMA-$P_{17.8}$ samples. Data indicate a progressive reduction of the P areal dose when increasing T_{ANN} for the PMMA-$P_{7.5}$ sample and an almost constant P areal dose for PMMA-$P_{17.8}$ irrespective of T_{ANN}. Considering that, according to NMR data, only one P-containing moiety is available for each PMMA chain and assuming that no thermal degradation of the PMMA-P polymers occurs during the grating process, the P areal dose measured by ToF-SIMS is indicative of the density of PMMA-P chains in the brush layer. The assumption of no degradation of the PMMA-P polymers is clearly supported by the MALDI analysis of the annealed samples that is reported in the Supporting Information. In this picture, each P atom that is detected by ToF-SIMS analysis in the δ-layer is considered as a tracer of a PMMA chain grafted over the Si substrate. As a

https://doi.org/10.1021/acsapm.1c01157
ACS Appl. Polym. Mater. 2021, 3, 6383−6393

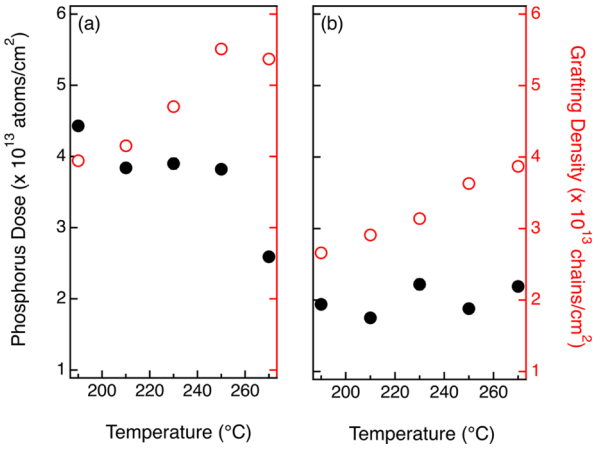

Figure 6. Measured P areal doses (closed black symbols) and calculated grafting densities (open red symbols) as a function of the annealing temperature (T_{ANN}) for the PMMA-$P_{7.5}$ (a) and PMMA-$P_{17.8}$ (b) samples, respectively. The samples were annealed for 900 s at T_{ANN} ranging from 190 to 270 °C.

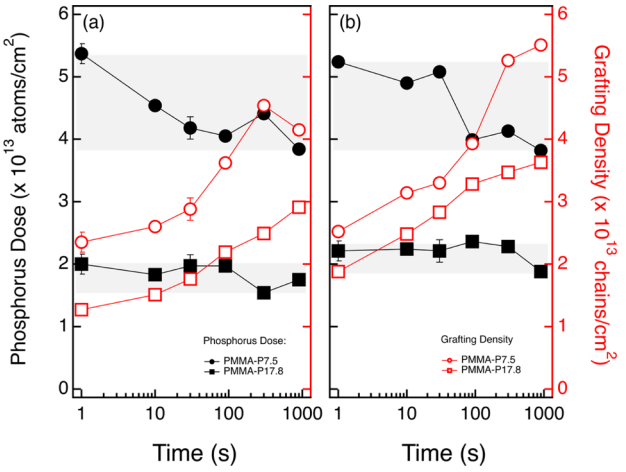

Figure 7. Evolution of P areal dose in the δ-layers as a function of t_{ANN} for the PMMA-$P_{7.5}$ (closed black circles) and PMMA-$P_{17.8}$ (closed black squares) samples at different T_{ANN} values, corresponding to 210 (a) and 250 °C (b), respectively. The bright dark areas highlight the variability range of the P areal dose in the δ-layers for the PMMA-$P_{7.5}$ and PMMA-$P_{17.8}$ samples. The evolution of the grafting density in the corresponding brush layers as function of time at 210 (a) and 250 °C (b) is reported as well.

consequence, counting the number of P atoms in the δ-layer, we obtain a direct indication of the number of polymer chains that are grafted on the surface of the sample. In other words, the P areal dose measured by ToF-SIMS is assumed to be equal to the effective grafting density (Σ_P) of the PMMA-P chains in the brush layer. Accordingly, experimental data indicate a progressive reduction of the effective grafting density in the brush layer when increasing T_{ANN} for PMMA-$P_{7.5}$ sample and an almost constant effective grafting density in the brush layer for PMMA-$P_{17.8}$ irrespective of T_{ANN}. Usually, the grafting density (Σ) in a brush layer is calculated according to the following equation

$$\Sigma = (HN_A\rho)/M_n \quad (1)$$

where H is the thickness of the brush layer, N_A is Avogadro's number, and ρ is the density of PMMA-P.[56] This equation assumes that the average molecular weight of the polymer in the grafted layer corresponds to the one in the pristine material. According to eq 1, the grafting density Σ is expected to linearly increase with H. Σ values for the PMMA-$P_{7.5}$ and PMMA-$P_{17.8}$ samples at different temperatures have been calculated by means of eq 1, considering the H values that have been measured by ellipsometry (Figure 3). The calculated Σ values (open red symbols) are reported as a function of the annealing temperature in Figure 6a,b for PMMA-$P_{7.5}$ and PMMA-$P_{17.8}$ samples, respectively. A progressive increase of Σ is observed when increasing T_{ANN}. Conversely, P areal dose measurements suggest a completely different scenario for the effective grafting density Σ_P. In particular, for PMMA-$P_{7.5}$, a progressive reduction of the effective grafting density Σ_P is observed when increasing T_{ANN}, corresponding to a continuous decrease of Σ_P when increasing thickness H of the brush layer.

Similarly, Figure 7a,b shows the evolution of P areal dose in the δ-layers as a function of t_{ANN} for the PMMA-$P_{7.5}$ (closed black circles) and PMMA-$P_{17.8}$ (closed black squares) samples at different T_{ANN} values, corresponding to 210 and 250 °C, respectively. A significant decrease in the P areal dose with time is observed in the case of PMMA-$P_{7.5}$, irrespective of the annealing temperature T_{ANN}. In the case of PMMA-$P_{17.8}$, the P areal dose is almost constant, exhibiting a quite limited reduction for very long annealing time t_{ANN}. The Σ values calculated from eq 1 as a function of t_{ANN} for the PMMA-$P_{7.5}$ (open red circles) and PMMA-$P_{17.8}$ (open red squares) samples at T_{ANN} = 210 °C and T_{ANN} = 250 °C are also reported in Figure 6a,b and set forth a growth of the grafting density with t_{ANN}. Once again, the P areal dose data indicate a completely different evolution of the effective grafting density Σ_P during the "grafting to" process. In particular, for very short t_{ANN} values, the effective grafting density Σ_P values are systematically higher than the Σ values that have been calculated using eq 1. Moreover, Σ_P values follow an inverse trend as a function of time with respect to the one expected on the basis of the evolution of the thickness H. It is worth to remind that eq 1 is expected to provide a reliable evaluation of the grafting density of a polymer with molecular weight M_n in the polymer brush with thickness H, assuming that the average molecular weight of the polymer chains in the brush layer is equal to the one in the as-synthesized polymer sample. In contrast, Σ_P values suggest that the effective mass distributions in grafted layers are different from the one of the original polymer sample.

Polymer Mass Distribution. To countercheck the ToF-SIMS data, the polymer mass distribution in the PMMA-$P_{7.5}$ brush layer was investigated by MALDI-TOF analysis of the unreacted PMMA-$P_{7.5}$ chains. After the spin-coating process on silicon wafers and the thermally promoted grafting reaction, the fractions of unreacted PMMA-$P_{7.5}$ chains were collected during the toluene washing process and analyzed by using a MALDI-TOF mass spectrometer. The acquired mass distributions were then compared with the *zero-time* mass distribution, obtained from a sample in which PMMA-$P_{7.5}$ was spin-coated onto nondeglazed Si substrates and then recovered without any thermal treatments, taking into account the specific fragmentation behavior of PMMA chains prepared by ATRP.[57−60] A detailed discussion of the collected spectra is reported in the Supporting Information. To obtain information about the grafting process effect on the molecular weight distribution, the overall MALDI-TOF spectrum of the

https://doi.org/10.1021/acsapm.1c01157
ACS Appl. Polym. Mater. 2021, 3, 6383−6393

unreacted PMMA-$P_{7.5}$ chains relative to each sample was divided into two parts, defined by the m/z value relative to the maximum of the overall distribution in the zero-time sample. The integral of the peaks on the left of the critical m/z value was defined as a *low-molecular-weight area* and the integral on the right as *high-molecular-weight area*. The ratio between the value relative to the *low-molecular-weight area* on the sum of *low* and *high mass areas* was defined as f_{SMA}.

Figure 8 reports the values of f_{SMA} for the samples annealed for 1, 30, 90, and 900 s at 250 °C and at various temperatures

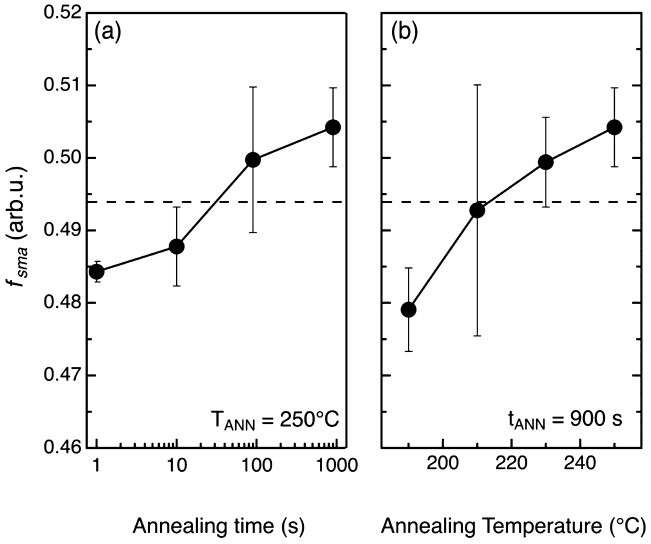

Figure 8. Ratio f_{SMA} between the value relative to the low molecular weight area and the total area of the MALDI-TOF spectra of the unreacted PMMA-$P_{7.5}$ chains for the samples annealed for 1, 10, 30, and 900 s at 250 °C (a) and at 190, 210, 230, and 250 °C for 900 s (b), respectively. The dashed line indicates the value of f_{SMA} in the not annealed sample.

for 900 s. The dotted line points the value of f_{SMA} in the zero-time sample. For short annealing time and relatively low temperature, a reduction of low-molecular-weight component in the unreacted PMMA-$P_{7.5}$ chains is observed, demonstrating that an enrichment of low molecular weights occurs in the grafted brush during the initial stages of the "grafting to" process. However, for a longer grafting time and higher temperature, the value of f_{SMA} increases, demonstrating that the average molecular weight of the grafted polymers increases, reaching values slightly higher than the corresponding values of the zero-time sample. Although this analysis is purely qualitative due to the well-known molecular weight discrimination of the MALDI-TOF,[61] the data indicate that for short annealing time or low temperature, the lower molecular weight species are preferentially grafted to the substrate surface. However, corresponding to longer annealing time or higher temperature, the average molecular weight of the grafted brush increases in agreement with the trend of the dopant atom amount.

DISCUSSION

Collected data provide significant information about the "grating to" process from the melt and suggest that current models describing the "grafting to" process does not fully account for the evolution, as a function of time, of the grafting density of the PMMA-P polymer chains in the brush layer. According to the conventional model proposed by Kramer,[39] in the classical diffusion limited regime, the thickness of the brush layer increases with the logarithm of the processing time due to the progressive anchoring of the end-functionalized polymer chains to the substrate. When the thickness of the brush layer is approximately 2 times the radius of gyration of the polymer, the classical diffusion limited regime turns into a penetration limited regime. Transition is due to a potential barrier of entropic nature that prevents the penetration of nongrafted chains into the brush as a consequence of the significant stretching of the anchored chains that is required to accommodate the incoming ones. As a consequence, the brush thickness gets to a pseudo-plateau value, making the grafting reaction an almost self-limiting reaction.[39] When operating at high temperatures, a significant speed up of the "grafting to" process from melt has been observed.[44] Despite the faster diffusion kinetics at a high temperature, no effective variation of the final pseudo-plateau thickness value has been reported. This fact suggests that no relevant changes of the entropic barrier have occurred in the range of temperatures that has been investigated.[51]

In this framework, the grafting density is expected to progressively increase with time and a linear correlation between grafting density and thickness is expected to hold according to eq 1. Conversely, the P areal doses measured by ToF-SIMS indicate that the effective grafting density Σ_P of the PMMA-P chains in the brush layer progressively decreases with time, following an opposite trend compared to the one predicted by the conventional model. It is worth to note that the determination of the grafting density by means of eq 1 implicitly assumes that the molecular weight characteristics of the original polymeric material perfectly correspond to those of the surface-tethered polymers. However, recent experiments for the "grafting to" process from solution unambiguously established the preferred surface grafting of shorter polymers, which can be correlated to their smaller radius of gyration.[41,42] The experimental results reported by Michalek et al. demonstrated and quantified the distortion of the polymer mass distribution when grafted from solution onto a surface. This distortion critically affects the methods for the determination of the grafting density that rely on information about the average molecular weight of the grafted polymer obtained from the analysis of the bulk material. According to these results, the discrepancy between the values of the grafting density Σ calculated from eq 1 and the values of the effective grafting density Σ_P obtained from ToF-SIMS measurements can be rationalized assuming that, in this specific system, the molecular weight distribution of the surface-tethered polymers does not perfectly match the one of the original polymeric material.

Actually, eq 1 is intrinsically correct, as it comes from stoichiometry considerations, and properly describes the correlation between the effective grafting density of the polymer chains in the brush layer and the average molecular weight of the grafted polymer chains. Accordingly, instead of determining the grafting density from the brush layer thickness and the average molecular weight of the bulk polymer, eq 1 can be used to estimate the average molecular weight of the grafted polymer by combining the brush layer thickness values obtained by ellipsometry and the effective grafting density Σ_P of the PMMA-P chains, which is assumed to be equal to the P areal density determined by TOF SIMS experiments. Figure 9a,b shows the evolution of the average molecular weight of

https://doi.org/10.1021/acsapm.1c01157
ACS Appl. Polym. Mater. 2021, 3, 6383−6393

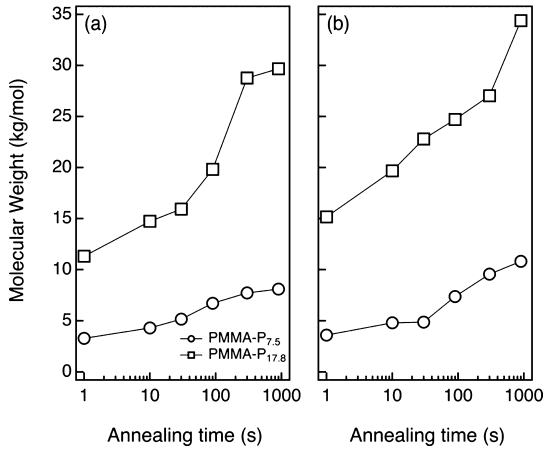

Figure 9. Evolution as a function of t_{ANN} of the average molecular weight of the polymeric chains in the brush layer for PMMA-$P_{7.5}$ (open black circles) and PMMA-$P_{17.8}$ (open black squares) at different T_{ANN} values, corresponding to 210 (a) and 250 °C (b), respectively.

the PMMA-P chains in the brush layer as a function of t_{ANN} for the PMMA-$P_{7.5}$ (open black circles) and PMMA-$P_{17.8}$ (open black squares) samples at different T_{ANN} values, corresponding to 210 and 250 °C, respectively. The values of the average molecular weight of the PMMA-P chains in the brush layer fall well within the range of molecular weight values defined by the molecular weight distributions of the pristine PMMA-$P_{7.5}$ and PMMA-$P_{17.8}$ samples that are reported in Figure 1. According to the data reported in Figure 9, during the initial stages of the "grafting to" process, the average molecular weight of the polymer chains is much lower than in the initial polymer distribution, supporting the idea of a preferential grafting of the short polymer chains over the long ones. The average molecular weight of the PMMA-P progressively increases with time, suggesting the occurrence of an efficient exchange mechanism between high-molecular-weight chains in the melt and low-molecular-weight ones tethered to the substrate, in agreement with recent experimental results.[40] Collected experimental data suggest that short polymer chains graft first, forming, during the initial stages of the grafting process, a thin brush layer characterized by high grafting density values. The progressive decrease of the effective grafting density with time is attributed to the subsequent grafting of long polymer chains that replace the short polymers forming a thick brush layer with a low grafting density. The effect is more evident in the case of the PMMA-$P_{7.5}$ sample because at low molecular weight, a small variation in the average molecular weight of the grafted polymer chains corresponds to a large variation of the grafting density.

The preferential attachment of short over long polymer chains during the initial stages of the grafting process appears possible due to diffusion, probability, and geometrical effects, in perfect agreement with data reported by Michalek et al. in the case of "grafting to" from solution.[41] In the case of "grafting to" from melt, additional effects have to be taken into account. Several papers reported about the segregation of short chains at the surface of the polymeric film and at the interface with the underlying substrate. In particular, theoretical investigations indicate that in the absence of preferential interactions between monomers and the interface, enhancement of the chain end density within a distance of approximately two polymer segment lengths of the interface relative to the bulk is expected due to the segregation phenomena that are determined by minimization of the loss of conformational entropy near an impenetrable boundary.[62] Hill et al. showed that the entropically driven surface enrichment of shorter chains occurs even in low polydispersity materials and that the shift in M_n from bulk to surface is larger for PMMA than for the somewhat stiffer PS chains.[63,64] Segregation effects could be even stronger in the case of end-functionalized polymer chains because the enthalpic interactions that control surface/interface attraction are often much stronger than any entropic effects.[65] All these studies suggest that the segregation of short polymer chains at the interface between the PMMA-P thin film and the underlying nondeglazed Si substrate could play a role in the enrichment of short PMMA-P chains that is observed during the initial stages of the grafting process. Present data indicate that the kinetic and mechanism of the grafting to process are much more complex than expected according to the conventional models and deserve further studies to be fully understood.

From the point of view of the target application, these data highlight that, even taking into account all these phenomena, the proposed approach guarantees a high level of control on the dopant concentration in the δ-layer. In previous papers, Perego et al. showed excellent control of the doping level in silicon substrates by means of thermal diffusion of P atoms from dopant sources created via grafting of phosphorus end-terminated polymers.[27,29,30] The proposed doping approach relies on the main assumption that, taking advantage of the self-limiting nature of the "grafting to" process from the melt, proper selection of the polymer M_n guarantees precise control of the areal dose and spatial distribution of dopants. Present work indicates that the effective grafting density of the polymer chains onto the Si substrate is not fully controlled by the selection of the M_n, but it is somehow affected by the polydispersity of the phosphorus end-terminated polymers that are used to create the brush layer. Actually, variations of the dopant concentration as a function of processing time and temperature are quite limited with an average P dose of $4.5 \times 10^{13} \pm 0.5 \times 10^{13}$ atoms/cm^2 for PMMA-$P_{7.5}$ and $2.0 \times 10^{13} \pm 0.3 \times 10^{13}$ atoms/cm^2 for PMMA-$P_{17.8}$, respectively, as highlighted by the bright dark areas in Figure 6. Despite the variability introduced by these polydispersity-related effects, the collected data demonstrate that the effective amount of P atoms in the δ-layer is essentially determined by the molecular weight of the PMMA-P polymer. In this respect, the effects that are herein reported determine limited variations of the P dose and, from this point of view, can be regarded as second-order effects associated to polydispersity of the P-terminated polymers. As a consequence, accurate tuning of the processing conditions is requested to guarantee precise control of the P areal dose. Nevertheless, the collected data highlight that the doping process is robust and highly reproducible, offering the possibility to properly adjust the effective P dose in the P δ-layer by controlling the processing parameters for a P-terminated polymer with a specific M_n value.

From another point of view, these second-order effects associated to the polydispersity of the P-terminated polymer introduce a certain degree of uncertainty in the grafting density of the polymer chains within the brush layer and prevent the possibility to achieve deterministic control of the dopant dose in the P δ-layer. Although the PMMA-P samples were prepared by a controlled polymerization process leading to samples

https://doi.org/10.1021/acsapm.1c01157
ACS Appl. Polym. Mater. 2021, 3, 6383−6393

featuring a relatively narrow polydispersity index, the difference in chain length revealed sufficiently pronounced to promote the observed partitioning during the "grafting to" process. Consequently, precise polymerization strategies are necessary to achieve the level of control that is required to attain the goal of deterministic doping. In particular, precise polymerization technology could provide polymers with absolute control over chain length.[66−68] Polymers terminated with dopant-containing moieties and deterministically controlled degree of polymerization are envisioned as the final solution to develop an effective technology platform for deterministic doping.

CONCLUSIONS

PMMA samples terminated with a P-containing moiety and narrow molecular weight distributions have been used to produce P δ-layers in a SiO_2 matrix, in view of their potential application as sources of impurity atoms for the doping of the underlying Si substrate. The concentration of P atoms in the different δ-layers has been monitored with respect to the molecular weight of the P-terminated polymer and the processing parameters, that is, time and temperature of the thermal treatment that is used to form the brush layer by anchoring of the P-terminated polymers onto the nondeglazed Si substrate. The P dose in the δ-layer is mostly determined by the specific molecular weight of the P-terminated polymer. However, limited but systematic variations in the P dose are observed when changing the processing parameters, with a progressive reduction as a function of the annealing time. This experimental finding suggests that a distortion of the molecular weight distribution of the grafted species with respect to the initial polymer takes place during the "grafting to" process. The overall picture of the experimental data confirms that the "grafting to" process represents a robust and highly reproducible approach for the synthesis of dopant sources because the effective P dose in the P δ-layer is adjusted by the proper selection of the molecular weight of the P-terminated PMMA, provided that tight control over the processing parameters is exercised. Nevertheless, reported data indicate that to achieve deterministic control of the dose of dopants in the P δ-layer, precise polymers would be highly desirable. Additionally, these results depict an interesting scenario about the mechanism governing the "grafting to" process of P-terminated PMMA polymers that deserves further investigations to be fully understood.

ASSOCIATED CONTENT

Supporting Information

The Supporting Information is available free of charge at https://pubs.acs.org/doi/10.1021/acsapm.1c01157.

^{1}H NMR and ^{13}C NMR spectra of PMMA-$OH_{5.6}$ and PMMA-$P_{7.5}$ samples, ^{31}P NMR spectrum of the PMMA-$P_{7.5}$ sample, MALDI-TOF MS spectrum of the PMMA-$P_{7.5}$ sample, and SEM images of PMMA-$P_{7.5}$ samples (PDF)

AUTHOR INFORMATION

Corresponding Authors

Michele Perego − *IMM-CNR Agrate Unit, I-20864 Agrate Brianza, Italy*; orcid.org/0000-0001-7431-1969; Email: michele.perego@cnr.it

Michele Laus − *Università del Piemonte Orientale "A. Avogadro", I-15121 Alessandria, Italy*; Email: michele.laus@uniupo.it

Authors

Stefano Kuschlan − *IMM-CNR Agrate Unit, I-20864 Agrate Brianza, Italy; Università del Piemonte Orientale "A. Avogadro", I-15121 Alessandria, Italy*

Gabriele Seguini − *IMM-CNR Agrate Unit, I-20864 Agrate Brianza, Italy*; orcid.org/0000-0002-7729-6212

Riccardo Chiarcos − *IMM-CNR Agrate Unit, I-20864 Agrate Brianza, Italy; Università del Piemonte Orientale "A. Avogadro", I-15121 Alessandria, Italy*

Valentina Gianotti − *Università del Piemonte Orientale "A. Avogadro", I-15121 Alessandria, Italy*; orcid.org/0000-0001-7273-4474

Diego Antonioli − *Università del Piemonte Orientale "A. Avogadro", I-15121 Alessandria, Italy*

Katia Sparnacci − *Università del Piemonte Orientale "A. Avogadro", I-15121 Alessandria, Italy*

Complete contact information is available at: https://pubs.acs.org/10.1021/acsapm.1c01157

Notes

The authors declare no competing financial interest.

ACKNOWLEDGMENTS

The authors acknowledge M. Alia (CNR) for his collaboration during the processing of the sample in a clean room and his support with the e-beam evaporation system.

REFERENCES

(1) Chaki, N. K.; Vijayamohanan, K. Self-Assembled Monolayers as a Tunable Platform for Biosensor Applications. *Biosens. Bioelectron.* **2002**, *17*, 1−12.

(2) Weng, Z.; Zaera, F. Increase in Activity and Selectivity in Catalysis via Surface Modification with Self-Assembled Monolayers. *J. Phys. Chem. C* **2014**, *118*, 3672−3679.

(3) Senaratne, W.; Andruzzi, L.; Ober, C. K. Self-Assembled Monolayers and Polymer Brushes in Biotechnology:Current Applications and Future Perspectives. *Biomacromolecules* **2005**, *6*, 2427−2448.

(4) Lin, Y.; Firdaus, Y.; Isikgor, F. H.; Nugraha, M. I.; Yengel, E.; Harrison, G. T.; Hallani, R.; El-Labban, A.; Faber, H.; Ma, C.; Zheng, X.; Subbiah, A.; Howells, C. T.; Bakr, O. M.; McCulloch, I.; Wolf, S. D.; Tsetseris, L.; Anthopoulos, T. D. Self-Assembled Monolayer Enables Hole Transport Layer-Free Organic Solar Cells with 18% Efficiency and Improved Operational Stability. *ACS Energy Lett.* **2020**, *5*, 2935−2944.

(5) Liu, D.; Miao, Q. Recent Progress in Interface Engineering of Organic Thin Film Transistors with Self-Assembled Monolayers. *Mater. Chem. Front.* **2018**, *2*, 11−21.

(6) Cattani-Scholz, A. Functional Organophosphonate Interfaces for Nanotechnology: A Review. *ACS Appl. Mater. Interfaces* **2017**, *9*, 25643−25655.

(7) Lecollinet, G.; Delorme, N.; Edely, M.; Gibaud, A.; Bardeau, J.-F.; Hindré, F.; Boury, F.; Portet, D. Self-Assembled Monolayers of Bisphosphonates: Influence of Side Chain Steric Hindrance. *Langmuir* **2009**, *25*, 7828−7835.

(8) Cattani-Scholz, A.; Liao, K.-C.; Bora, A.; Pathak, A.; Hundschell, C.; Nickel, B.; Schwartz, J.; Abstreiter, G.; Tornow, M. Molecular Architecture: Construction of Self-Assembled Organophosphonate Duplexes and Their Electrochemical Characterization. *Langmuir* **2012**, *28*, 7889−7896.

(9) Davidowski, S. K.; Holland, G. P. Solid-State NMR Characterization of Mixed Phosphonic Acid Ligand Binding and Organization on Silica Nanoparticles. *Langmuir* **2016**, *32*, 3253−3261.
(10) Vega, A.; Thissen, P.; Chabal, Y. J. Environment-Controlled Tethering by Aggregation and Growth of Phosphonic Acid Monolayers on Silicon Oxide. *Langmuir* **2012**, *28*, 8046−8051.
(11) Auzelle, T.; Ullrich, F.; Hietzschold, S.; Sinito, C.; Brackmann, S.; Kowalsky, W.; Mankel, E.; Brandt, O.; Lovrincic, R.; Fernández-Garrido, S. External Control of GaN Band Bending Using Phosphonate Self-Assembled Monolayers. *ACS Appl. Mater. Interfaces* **2021**, *13*, 4626−4635.
(12) Auernhammer, M.; Schoell, S. J.; Sachsenhauser, M.; Liao, K.-C.; Schwartz, J.; Sharp, I. D.; Cattani-Scholz, A. Surface Functionalization of 6H-SiC Using Organophosphonate Monolayers. *Appl. Phys. Lett.* **2012**, *100*, 101601.
(13) Raynor, J. E.; Capadona, J. R.; Collard, D. M.; Petrie, T. A.; García, A. J. Polymer Brushes and Self-Assembled Monolayers: Versatile Platforms to Control Cell Adhesion to Biomaterials (Review). *Biointerphases* **2009**, *4*, FA3−FA16.
(14) Wilkins, S. J.; Slomski, M. J.; Paskova, T.; Weyher, J. L.; Ivanisevic, A. Modulated Optical Sensitivity with Nanostructured Gallium Nitride. *Appl. Phys. Lett.* **2015**, *106*, 151602.
(15) Ho, J. C.; Yerushalmi, R.; Jacobson, Z. A.; Fan, Z.; Alley, R. L.; Javey, A. Controlled Nanoscale Doping of Semiconductors via Molecular Monolayers. *Nat. Mater.* **2008**, *7*, 62−67.
(16) Ho, J. C.; Yerushalmi, R.; Smith, G.; Majhi, P.; Bennett, J.; Halim, J.; Faifer, V. N.; Javey, A. Wafer-Scale, Sub-5 Nm Junction Formation by Monolayer Doping and Conventional Spike Annealing. *Nano Lett.* **2009**, *9*, 725−730.
(17) Longo, R. C.; Cho, K.; Schmidt, W. G.; Chabal, Y. J.; Thissen, P. Monolayer Doping via Phosphonic Acid Grafting on Silicon: Microscopic Insight from Infrared Spectroscopy and Density Functional Theory Calculations. *Adv. Funct. Mater.* **2013**, *23*, 3471−3477.
(18) Csiki, R.; Parzinger, E.; Stutzmann, M.; Wurstbauer, U.; Cattani-Scholz, A.; Schwartz, J. Tuning the Physical Properties of MoS2 Membranes through Organophosphonate Interfacial Chemistry. In *2015 IEEE 15th International Conference on Nanotechnology*; IEEE-NANO, 2015; pp 1564−1567.
(19) Zhang, C.; Chang, S.; Dan, Y. Advances in Ultrashallow Doping of Silicon. *Adv. Phys.: X* **2021**, *6*, 1871407.
(20) Zhang, C.; Li, K.; Zang, X.; Ma, F.; Dan, Y. Towards Fabrication of Atomic Dopant Wires via Monolayer Doping Patterned by Resist-Free Lithography. *Chin. Phys. Lett.* **2021**, *38*, 028101.
(21) Gao, X.; Guan, B.; Mesli, A.; Chen, K.; Dan, Y. Deep Level Transient Spectroscopic Investigation of Phosphorus-Doped Silicon by Self-Assembled Molecular Monolayers. *Nat. Commun.* **2018**, *9*, 118.
(22) Caccamo, S.; Puglisi, R. A.; Di Franco, S.; D'Urso, L.; Indelicato, V.; Italia, M.; Pannitteri, S.; La Magna, A. Silicon Doped by Molecular Doping Technique: Role of the Surface Layers of Doped Si on the Electrical Characteristics. *Mater. Sci. Semicond. Process.* **2016**, *42*, 200−203.
(23) Gianotti, V.; Antonioli, D.; Sparnacci, K.; Laus, M.; Cassino, C.; Marsano, F.; Seguini, G.; Perego, M. TGA-GC−MS Quantitative Analysis of Phosphorus-End Capped Functional Polymers in Bulk and Ultrathin Films. *J. Anal. Appl. Pyrolysis* **2017**, *128*, 238−245.
(24) Hazut, O.; Agarwala, A.; Amit, I.; Subramani, T.; Zaidiner, S.; Rosenwaks, Y.; Yerushalmi, R. Contact Doping of Silicon Wafers and Nanostructures with Phosphine Oxide Monolayers. *ACS Nano* **2012**, *6*, 10311−10318.
(25) Arduca, E.; Mastromatteo, M.; Salvador, D. D.; Seguini, G.; Lenardi, C.; Napolitani, E.; Perego, M. Synthesis and Characterization of P δ-Layer in SiO\\textlessinf\\textgreater2\\textless/Inf\\textgreater by Monolayer Doping. *Nanotechnology* **2016**, *27*, 075606.
(26) O'Connell, J.; Collins, G.; McGlacken, G. P.; Duffy, R.; Holmes, J. D. Monolayer Doping of Si with Improved Oxidation Resistance. *ACS Appl. Mater. Interfaces* **2016**, *8*, 4101−4108.
(27) Perego, M.; Seguini, G.; Arduca, E.; Nomellini, A.; Sparnacci, K.; Antonioli, D.; Gianotti, V.; Laus, M. Control of Doping Level in Semiconductors via Self-Limited Grafting of Phosphorus End-Terminated Polymers. *ACS Nano* **2018**, *12*, 178−186.
(28) Chiarcos, R.; Gianotti, V.; Cossi, M.; Zoccante, A.; Antonioli, D.; Sparnacci, K.; Laus, M.; Caligiore, F. E.; Perego, M. Thermal Degradation in Ultrathin Films Outperforms Dose Control of N-Type Polymeric Dopants for Silicon. *ACS Appl. Electron. Mater.* **2019**, *1*, 1807−1816.
(29) Perego, M.; Caruso, F.; Seguini, G.; Arduca, E.; Mantovan, R.; Sparnacci, K.; Laus, M. Doping of Silicon by Phosphorus End-Terminated Polymers: Drive-in and Activation of Dopants. *J. Mater. Chem. C* **2020**, *8*, 10229−10237.
(30) Perego, M.; Seguini, G.; Mascheroni, E.; Arduca, E.; Gianotti, V.; Laus, M. Doping of Silicon with Phosphorus End-Terminated Polymers: Source Characterization and Dopant Diffusion in SiO2. *J. Mater. Chem. C* **2021**, *9*, 4020−4028.
(31) Hoarfrost, M. L.; Takei, K.; Ho, V.; Heitsch, A.; Trefonas, P.; Javey, A.; Segalman, R. A. Spin-On Organic Polymer Dopants for Silicon. *J. Phys. Chem. Lett.* **2013**, *4*, 3741−3746.
(32) Popere, B. C.; Russ, B.; Heitsch, A. T.; Trefonas, P.; Segalman, R. A. Large-Area, Nanometer-Scale Discrete Doping of Semiconductors via Block Copolymer Self-Assembly. *Adv. Mater. Interfaces* **2015**, *2*, 1500421.
(33) Katsumata, R.; Limary, R.; Zhang, Y.; Popere, B. C.; Heitsch, A. T.; Li, M.; Trefonas, P.; Segalman, R. A. Mussel-Inspired Strategy for Stabilizing Ultrathin Polymer Films and Its Application to Spin-On Doping of Semiconductors. *Chem. Mater.* **2018**, *30*, 5285−5292.
(34) Wu, H.; Guan, B.; Sun, Y.; Zhu, Y.; Dan, Y. Controlled Doping by Self-Assembled Dendrimer-like Macromolecules. *Sci. Rep.* **2017**, *7*, 41299.
(35) Chen, W.-L.; Cordero, R.; Tran, H.; Ober, C. K. 50th Anniversary Perspective: Polymer Brushes: Novel Surfaces for Future Materials. *Macromolecules* **2017**, *50*, 4089−4113.
(36) Solimando, X.; Kennedy, E.; David, G.; Champagne, P.; Cunningham, M. F. Phosphorus-Containing Polymers Synthesised via Nitroxide-Mediated Polymerisation and Their Grafting on Chitosan by Grafting to and Grafting from Approaches. *Polym. Chem.* **2020**, *11*, 4133−4142.
(37) Babu, K.; Dhamodharan, R. Grafting of Poly(Methyl Methacrylate) Brushes from Magnetite Nanoparticles Using a Phosphonic Acid Based Initiator by Ambient Temperature Atom Transfer Radical Polymerization (ATATRP). *Nanoscale Res. Lett.* **2008**, *3*, 109.
(38) Zhang, S.; Vi, T.; Luo, K.; Koberstein, J. T. Kinetics of Polymer Interfacial Reactions: Polymer Brush Formation by Click Reactions of Alkyne End-Functional Polymers with Azide-Functional Substrates. *Macromolecules* **2016**, *49*, 5461−5474.
(39) Kramer, E. J. Grafting Kinetics of End-Functional Polymers at Melt Interfaces. *Isr. J. Chem.* **1995**, *35*, 49−54.
(40) Laus, M.; Chiarcos, R.; Gianotti, V.; Antonioli, D.; Sparnacci, K.; Munaò, G.; Milano, G.; De Nicola, A.; Perego, M. Evidence of Mechanochemical Control in "Grafting to" Reactions of Hydroxy-Terminated Statistical Copolymers. *Macromolecules* **2021**, *54*, 499−508.
(41) Michalek, L.; Mundsinger, K.; Barner-Kowollik, C.; Barner, L. The Long and the Short of Polymer Grafting. *Polym. Chem.* **2019**, *10*, 54−59.
(42) Michalek, L.; Mundsinger, K.; Barner, L.; Barner-Kowollik, C. Quantifying Solvent Effects on Polymer Surface Grafting. *ACS Macro Lett.* **2019**, *8*, 800−805.
(43) Lundy, R.; Yadav, P.; Prochukhan, N.; Giraud, E. C.; O'Mahony, T. F.; Selkirk, A.; Mullen, E.; Conway, J.; Turner, M.; Daniels, S.; Mani-Gonzalez, P. G.; Snelgrove, M.; Bogan, J.; McFeely, C.; O'Connor, R.; McGlynn, E.; Hughes, G.; Cummins, C.; Morris, M. A. Precise Definition of a "Monolayer Point" in Polymer Brush Films for Fabricating Highly Coherent TiO2 Thin Films by Vapor-Phase Infiltration. *Langmuir* **2020**, *36*, 12394−12402.

https://doi.org/10.1021/acsapm.1c01157
ACS Appl. Polym. Mater. 2021, 3, 6383−6393

(44) Ferrarese Lupi, F.; Giammaria, T. J.; Seguini, G.; Ceresoli, M.; Perego, M.; Antonioli, D.; Gianotti, V.; Sparnacci, K.; Laus, M. Flash Grafting of Functional Random Copolymers for Surface Neutralization. *J. Mater. Chem. C* **2014**, *2*, 4909.
(45) Mastromatteo, M.; Arduca, E.; Napolitani, E.; Nicotra, G.; De Salvador, D.; Bacci, L.; Frascaroli, J.; Seguini, G.; Scuderi, M.; Impellizzeri, G.; Spinella, C.; Perego, M.; Carnera, A. Quantification of Phosphorus Diffusion and Incorporation in Silicon Nanocrystals Embedded in Silicon Oxide. *Surf. Interface Anal.* **2014**, *46*, 393−396.
(46) Perego, M.; Seguini, G.; Arduca, E.; Frascaroli, J.; De Salvador, D.; Mastromatteo, M.; Carnera, A.; Nicotra, G.; Scuderi, M.; Spinella, C.; Impellizzeri, G.; Lenardi, C.; Napolitani, E. Thermodynamic Stability of High Phosphorus Concentration in Silicon Nanostructures. *Nanoscale* **2015**, *7*, 14469.
(47) Ballard, D. G. H.; Wignall, G. D.; Schelten, J. Measurement of Molecular Dimensions of Polystyrene Chains in the Bulk Polymer by Low Angle Neutron Diffraction. *Eur. Polym. J.* **1973**, *9*, 965−969.
(48) Mansky, P.; Liu, Y.; Huang, E.; Russell, T. P.; Hawker, C. Controlling Polymer-Surface Interactions with Random Copolymer Brushes. *Science* **1997**, *275*, 1458.
(49) Jones, R. A. L.; Lehnert, R. J.; Schönherr, H.; Vancso, G. J. Factors affecting the preparation of permanently end-grafted polystyrene layers. *Polymer* **1999**, *40*, 525−530.
(50) Iyer, K. S.; Luzinov, I. Effect of Macromolecular Anchoring Layer Thickness and Molecular Weight on Polymer Grafting. *Macromolecules* **2004**, *37*, 9538−9545.
(51) Sparnacci, K.; Antonioli, D.; Gianotti, V.; Laus, M.; Ferrarese Lupi, F.; Giammaria, T. J.; Seguini, G.; Perego, M. Ultrathin Random Copolymer-Grafted Layers for Block Copolymer Self-Assembly. *ACS Appl. Mater. Interfaces* **2015**, *7*, 10944.
(52) Sparnacci, K.; Antonioli, D.; Gianotti, V.; Laus, M.; Zuccheri, G.; Ferrarese Lupi, F.; Giammaria, T. J.; Seguini, G.; Ceresoli, M.; Perego, M. Thermal Stability of Functional P(S-r-MMA) Random Copolymers for Nanolithographic Applications. *ACS Appl. Mater. Interfaces* **2015**, *7*, 3920.
(53) Michalek, L.; Barner, L.; Barner-Kowollik, C. Polymer on Top: Current Limits and Future Perspectives of Quantitatively Evaluating Surface Grafting. *Adv. Mater.* **2018**, *30*, 1706321.
(54) Holland, B. J.; Hay, J. N. The Effect of Polymerisation Conditions on the Kinetics and Mechanisms of Thermal Degradation of PMMA. *Polym. Degrad. Stab.* **2002**, *77*, 435−439.
(55) Ceresoli, M.; Palermo, M.; Ferrarese Lupi, F.; Seguini, G.; Perego, M.; Zuccheri, G.; Phadatare, S. D.; Antonioli, D.; Gianotti, V.; Sparnacci, K.; Laus, M. Neutral Wetting Brush Layers for Block Copolymer Thin Films Using Homopolymer Blends Processed at High Temperatures. *Nanotechnology* **2015**, *26*, 415603.
(56) Brittain, W. J.; Minko, S. A Structural Definition of Polymer Brushes. *J. Polym. Sci., Part A: Polym. Chem.* **2007**, *45*, 3505−3512.
(57) Singha, N. K.; Rimmer, S.; Klumperman, B. Mass Spectrometry of Poly(Methyl Methacrylate) (PMMA) Prepared by Atom Transfer Radical Polymerization (ATRP). *Eur. Polym. J.* **2004**, *40*, 159−163.
(58) Jackson, A. T.; Bunn, A.; Priestnall, I. M.; Borman, C. D.; Irvine, D. J. Molecular Spectroscopic Characterisation of Poly(Methyl Methacrylate) Generated by Means of Atom Transfer Radical Polymerisation (ATRP). *Polymer* **2006**, *47*, 1044−1054.
(59) Charles, L. MALDI of Synthetic Polymers with Labile End-Groups. *Mass Spectrom. Rev.* **2014**, *33*, 523−543.
(60) Iura, T.; Ohtani, H. Fragmentation Behavior of Poly(Methyl Methacrylate) during Matrix-Assisted Laser Desorption/Ionization. *Rapid Commun. Mass Spectrom.* **2015**, *29*, 155−162.
(61) Byrd, H. C. M.; McEwen, C. N. The Limitations of MALDI-TOF Mass Spectrometry in the Analysis of Wide Polydisperse Polymers. *Anal. Chem.* **2000**, *72*, 4568−4576.
(62) Zhao, W.; Zhao, X.; Rafailovich, M. H.; Sokolov, J.; Composto, R. J.; Smith, S. D.; Russell, T. P.; Dozier, W. D.; Mansfield, T.; Satkowski, M. Segregation of Chain Ends to Polymer Melt Surfaces and Interfaces. *Macromolecules* **1993**, *26*, 561−562.
(63) Hill, J. A.; Endres, K. J.; Mahmoudi, P.; Matsen, M. W.; Wesdemiotis, C.; Foster, M. D. Detection of Surface Enrichment Driven by Molecular Weight Disparity in Virtually Monodisperse Polymers. *ACS Macro Lett.* **2018**, *7*, 487−492.
(64) Hill, J. A.; Endres, K. J.; Meyerhofer, J.; He, Q.; Wesdemiotis, C.; Foster, M. D. Subtle End Group Functionalization of Polymer Chains Drives Surface Depletion of Entire Polymer Chains. *ACS Macro Lett.* **2018**, *7*, 795−800.
(65) Stein, G. E.; Laws, T. S.; Verduzco, R. Tailoring the Attraction of Polymers toward Surfaces. *Macromolecules* **2019**, *52*, 4787−4802.
(66) Patterson, A. L.; Danielsen, S. P. O.; Yu, B.; Davidson, E. C.; Fredrickson, G. H.; Segalman, R. A. Sequence Effects on Block Copolymer Self-Assembly through Tuning Chain Conformation and Segregation Strength Utilizing Sequence-Defined Polypeptoids. *Macromolecules* **2019**, *52*, 1277−1286.
(67) Song, Z.; Han, Z.; Lv, S.; Chen, C.; Chen, L.; Yin, L.; Cheng, J. Synthetic Polypeptides: From Polymer Design to Supramolecular Assembly and Biomedical Application. *Chem. Soc. Rev.* **2017**, *46*, 6570−6599.
(68) Lutz, J.-F.; Lehn, J.-M.; Meijer, E. W.; Matyjaszewski, K. From Precision Polymers to Complex Materials and Systems. *Nat. Rev. Mater.* **2016**, *1*, 16024.

https://doi.org/10.1021/acsapm.1c01157
ACS Appl. Polym. Mater. 2021, 3, 6383−6393